Coordination Chemistry Reviews 257 (2013) 2468–2483

Contents lists available at SciVerse ScienceDirect

Coordination Chemistry Reviews

journal homepage: www.elsevier.com/locate/ccr

Review

Sputtering deposition of nanoparticles onto liquid substrates: Recent advances and future trends

Heberton Wender[a,1], Pedro Migowski[b,1], Adriano F. Feil[c,1,2], Sérgio R. Teixeira[c], Jairton Dupont[b,*]

[a] Laboratório Nacional de Luz Síncrotron, R. Giuseppe Maximo Scolfaro, 10.000, P.O. Box 6192, CEP 13083-970 Campinas, Brazil
[b] Universidade Federal do Rio Grande do Sul, Instituto de Química, Av. Bento Goncalves, 9500, P.O. Box 15003, CEP 91501-970 Porto Alegre, RS, Brazil
[c] Universidade Federal do Rio Grande do Sul, Instituto de Física, Av. Bento Goncalves, 9500, P.O. Box 15051, 91501-970 Porto Alegre, RS, Brazil

Contents

ARTICLE INFO

Article history:
Received 13 November 2012
Received in revised form 2 January 2013
Accepted 9 January 2013
Available online 4 February 2013

Keywords:
Nanoparticles
Sputtering
Ionic liquids
Vegetable oils
Colloids

ABSTRACT

Nanoparticles (NPs) have recently attracted significant attention from the materials science community due to their promise to play an important role in developing new technologies. Indeed, NPs with small sizes, narrow size distributions and various shapes have been prepared via the reduction of organometallic compounds with molecular hydrogen, the decomposition of transition-metal complexes in the zero-valent state, metal bombardment or the simple transfer of previously prepared NPs from one liquid to another. This review paper will discuss the simple and quick method of sputtering deposition over liquid substrates to generate stable colloidal NPs. Initially, the sputtering phenomena will be presented in more detail, as well as the state-of-the-art in sputter deposition over both solid and liquid substrates. Then, special attention will be paid to sputtering onto ionic liquids (ILs), silicon oil and vegetable oils, and some selected results and the current mechanisms of NP formation will be discussed. Finally, applications of this new approach to synthesizing colloidal NPs will be shown.

* Corresponding author. Tel.: +55 5133086321; fax: +55 51 3332 6445.
E-mail address: jairton.dupont@ufrgs.br (J. Dupont).
[1] These authors contributed equally for this work.
[2] Present address: Energy Sciences, National Renewable Energy Laboratory, Golden, CO 80401, USA.

0010-8545/$ – see front matter © 2013 Elsevier B.V. All rights reserved.
http://dx.doi.org/10.1016/j.ccr.2013.01.013

1. Introduction

Nanoparticles (NPs), particles less than 100 nm in diameter, have recently attracted significant attention from the materials science community and promise to play an important role in the development of new technologies [1–4]. They exhibit unique physical properties that give rise to many potential applications in areas such as optics [5–7], luminescence [8–11], electronics [12–14], catalysis [15–20], solar energy conversion [21–23] and biomedicine [24–27]. Two fundamental factors, both related to the size of individual nanocrystals, are responsible for their properties. The first is the large surface to volume ratio, and the second factor is the quantum confinement effect.

Fundamentally, there are two general strategies whereby materials on the nanometric scale can be synthesized: chemical and physical methods. In the chemical methods, molecular species are transformed into nanoparticles. These methods can be divided into two major techniques: Chemical Vapor Deposition (CVD) with liquid phase synthesis and colloidal synthesis (CS). In the CVD process, the vaporized precursor compounds react in the gas phase, usually at high temperatures, and the nanostructures are obtained as powders or as films over substrates [28–31]. The control of the size of the materials in the CVD process is achieved by tuning the reaction parameters, such as temperature, flow rate and relative precursor quantities. On the other hand, the CS method is based on reactions between reactants in solution [1]. In this case, the size and shape of NPs are controlled via reaction conditions and stabilizing agents. In general, the CS of NPs has attracted more attention from the academic community than CVD due to its versatility. Furthermore, a wider range of applications is possible for NPs in solution.

As opposed to chemical procedures, the physical methods of nanostructure preparation are based on physical transformations of matter, which do not change the initial chemical composition. Using the physical methods, bulk materials are transformed into the nano scale via their interaction with photons, heat or ions or even by mechanical milling. In the case of photons, it is possible to highlight the laser-based techniques, such as laser ablation, Pulsed Laser Deposition (PLD) and laser-induced particle fragmentation [32]. In the second case, when matter is transformed by heat, the bulk material is evaporated and recrystallized on the nano scale [33]. On the other hand, as is implicit in its name, mechanical milling is based on milling the bulk particulate starting material until it is finely divided into nanometric particles. The transformation of matter via interaction with ions is based on the moment transfer between ions that collide on the surface of bulk materials, pulling out atoms or small clusters of the target material that are then directed to a substrate, where they begin to nucleate and grow. Here, the sputtering technique is highlighted [34].

Both chemical and physical methods have their advantages and can be complementary. Chemical synthesis is very versatile in terms of controlling NP size and enabling a variety of applications, but it usually generates harmful byproducts and NPs with limited purity. On the other hand, the physical methods are very clean methodologies to produce NPs, and the purity of the materials produced is the same as the starting material. Trying to combine both methodologies might open up a new way to synthesize NPs with controlled sizes, shapes and purities. In this scenario, sputtering deposition over a liquid substrate can be considered the most suitable method for giving rise to new and outstanding nanostructured materials [35,36].

This review paper will discuss the method of using sputtering deposition over liquid substrates in order to generate stable colloidal NPs. Initially, the sputtering phenomena will be presented in more detail, as well as state-of-the-art of the sputtering deposition over both solid and liquid substrates. Then, special attention will be paid to sputtering onto ionic liquids (ILs), silicon oil and vegetable oils, and some selected results will be discussed. Finally, applications regarding this new approach to synthesizing colloidal NPs will be shown.

2. Sputtering deposition

2.1. Physical fundaments of the sputtering process

Sputtering was first observed in a DC (Direct Current) gas discharge tube by Grove in 1852 [37]. He discovered that the cathode surface of the discharge tube was sputtered by energetic ions formed in the gas phase and that the cathode material was deposited on the inner wall of the discharge tube. Today, with the further development of this technique, it is well-known that in the sputtering deposition process, the bombardment of a target surface with energetic gaseous ions causes the physical ejection of surface atoms and/or small clusters, depending on the ions' incident energy. This technique is commonly used for thin-film deposition, etching and analytical techniques. There are different ways to perform sputtering, DC-diode, RF-diode (radio frequency) and magnetron sputtering being the three main processes.

In DC-diode sputtering, the difference in potential generated by a DC power supply will create an electrical field between the two electrodes, and in the presence of an inert gas, the ionization process occurs via electron collisions that form a plasma in the intermediate regions. This process occurs if there are satisfactory conditions, in terms of applied voltage and gas density, in the system.

However, in a DC-sputtering system, via the simple substitution of a metal target with an insulator target, the sputtering glow discharge cannot be sustained, because of the immediate build-up of a surface charge of positive ions on the front side of the insulator. To sustain the glow discharge with an insulator target, the DC power supply should be replaced with an RF power supply, and an impedance matching network should be implemented. This system is called RF-sputtering. Simple diode sputtering has two major problems: The deposition rate is slow, and the electron bombardment of the substrate is extensive and can cause overheating and structural damage.

Usually, sputtering sources are coupled with magnetrons that utilize strong magnetic fields to trap electrons close to target surface. The bombardment of a target surface by ions gives rise to a variety of elastic and inelastic collision events, leading to the ejection of a large variety of particles and the emission of radiation. Neutral atoms, as well as secondary ions, which are positively or negatively charged, and clusters (agglomerations of two or more atoms) are ejected.

Fig. 1a–c shows a representative sputtering system, in which the target and magnetrons, along with details, substrate positions, vacuum pumps, power supplies, plasma and the physical ejection of atoms from the target to the substrate surface, can be seen.

Due to the applied electric field, the electrons follow helical paths around the magnetic field lines, undergoing more ionizing collisions with gaseous neutrals near the target surface than would otherwise occur. However, as the sputtered atoms are neutrally charged, they are unaffected by the magnetic trap. Therefore, it is assumed that depending on the working pressure, the sputtered species experiences no considerable gas-phase collisions in the space between the target and the substrate. Stray magnetic fields leaking from the ferromagnetic targets also disturb the sputtering process. Specially designed sputter guns with unusually strong permanent magnets must often be used to compensate for this.

Another relevant factor in the sputtering process is the pressure in the vacuum chamber during deposition, which should be sufficiently low in order to pull the material out of the target and allow

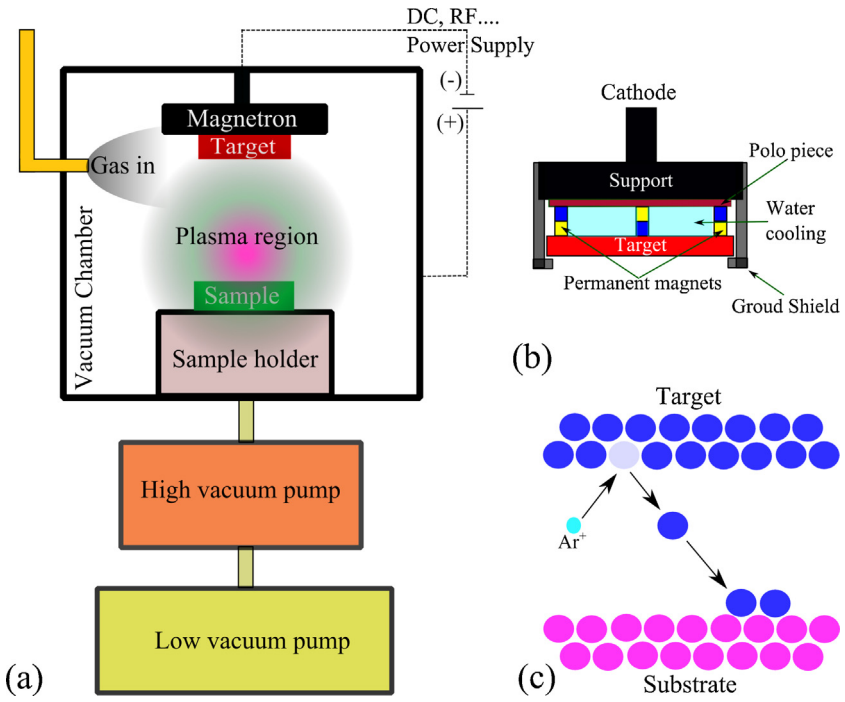

Fig. 1. (a) Representative scheme of a typical DC-magnetron sputtering system. (b) Details of the magnetron. (c) Representative scheme of the physical ejection of atoms from the target to the substrate surface.

it to reach the substrate without difficulty. On the other hand, the plasma collision between electrons and the atoms of neutral gases must be maintained. If the pressure is too low, the collision probability will diminish, hindering the maintenance of the plasma. The ideal pressure for the maintenance of the plasma inside the vacuum chamber is between 10^0 and 10^{-3} Pa. Therefore, vacuum pumps of different types are utilized in the sputtering systems so that they can work in low, high and ultrahigh vacuum conditions (see Fig. 1).

The more useful and practical parameters that control a sputtering process are the discharge voltage (V), discharge current (i), distance between the target and the substrate (d) and working pressure (P). By controlling these parameters, it is possible to control the sputtering rate, the velocity of the ejected atoms and their possible energy losses. The V and P parameters are directly related to the energy of the sputtered atoms (E), and d and P are related to the mean free path (λ) of the sputtered atoms by the equation $P \cdot d = \lambda$ [38]. Films with different characteristics can be obtained just by varying these parameters during a common sputtering process.

As an example, in the sputtering deposition of thin copper films onto silicon substrates, the sputtering power affected the structural properties of the copper films through the surface diffusion mechanism of ad atom [39]. In this case, a poor microstructure with voided boundaries is obtained as a result of the low sputtering power deposition, as is seen in the high resistivity. The deposition rate also depends on the deposition pressure. Deposition pressure has a contrary effect on the structural properties of copper films, in which a high deposition pressure favors the formation of a film structure with voided boundaries due to the shadowing effect, which varies with differing deposition pressures. Therefore, the control of all parameters during the sputtering process is fundamental to achieving the desired properties in the final product. Additionally, ZrO_2 films prepared via RF reactive sputtering using different substrate–target distances and RF powers show that the crystallite size increases as the substrate–target distance decreases and the RF power increases [40].

In general, sputtering is performed onto solid substrates, where the atoms nucleate and a film begins to grow after a few seconds. Models of thin film nucleation processes and other details can be seen in the sputtering deposition handbook [38]. However, it has recently been shown that sputtering can also be performed onto liquid substrates, for example, silicone oil [41], ILs [35,36] and vegetable oils [42]. Actually, this process can be performed on any liquid that has a sufficiently low vapor pressure to be introduced inside a vacuum.

2.2. Sputtering of metals onto liquid substrates: the beginning

The first sputtering deposition onto a liquid substrate was performed in 1996: the RF magnetron sputtering of silver directly onto pure silicone oil [43]. During the sputtering deposition process, a percolation structure appeared, and then, silver clusters formed on the oil surface, gradually grew and began to connect with one another. Finally, a continuous, rough, thin Ag film with a distinct surface morphology was formed. One should note an important result regarding this study: with a sputtering power lower than 30 W, a film could not be formed on the oil surface. Probably, Ag NPs were obtained inside the silicone oil; however, they were not identified and/or characterized, because the focus at the time was on obtaining a metallic film. The same authors found a significant difference between deposition rates onto a solid substrate and onto the liquid surface by simultaneously measuring the thickness of the film formed on the top of a glass substrate holding a silicone oil drop. They correlated this difference with secondary evaporation and penetration effects [44].

Although further investigations into film deposition onto the surface of silicone oil were carried out [45–58], it was only in 1999 when an innovative study was proposed by Wagener who described a versatile process to prepare magnetic colloidal solutions by using sputtering onto liquid surfaces [41]. For the first time, it was shown that metallic colloidal NPs could be obtained by sputtering deposition onto silicone oil. Nevertheless, silicone oil is not a good stabilizing agent, and the colloids obtained were not stable. To prevent agglomeration, it is very necessary to use

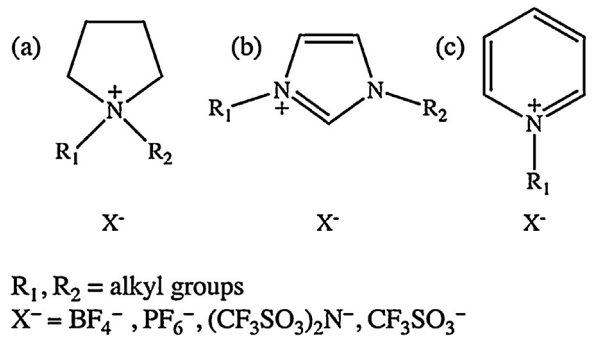

Fig. 2. Molecular structure of the ILs derived from the organic cations (a) N,N-dialkylpyrrolidinium, (b) 1,3-dialkylimidazolium and (c) N-alkylpyridinium.

another liquid substrate for the direct sputtering deposition of nanoparticles without the addition of stabilizers.

After these pioneering studies, in 2006, two groups performed the sputtering of metals onto ILs for two different applications: one for the deposition of metallic films onto IL as a basis for lunar telescopes [59] and other for the synthesis of stable colloidal metal nanoparticles [36] without using stabilizers. Both results initiated a series of efforts to understand the mechanism of nanoparticle formation through sputtering onto liquids. Table 1 summarizes some results obtained by sputtering onto liquid surfaces until 2006. The newest results regarding ILs and vegetable oils will be discussed in the next section, after a small introduction concerning ILs and the chemical synthesis of colloidal nanoparticles.

3. Chemical synthesis of nanoparticles in ionic liquids

3.1. Ionic liquids

ILs can generally be defined as liquid electrolytes composed entirely of ions. Currently, pure or eutectic mixtures of inorganic/organic salts that melt below 100 °C are considered to be ILs [60]. Although known since the early 1900s, the applications of ILs emerged in the 1990s due to the advent of the synthesis of air- and water-stable room-temperature ILs. Among all known ILs, the ones that show the most attractive physico-chemical properties are the organic salts derived from 1,3-dialkylimidazolium, N,N-dialkylpyrrolidinium and N-alkylpyridinium cations, as shown in Fig. 2. It is possible to highlight their wide electrochemical windows, good ionic conductivity [61], low vapor pressures and excellent thermal and chemical stabilities [60].

The potential of these compound classes was first exploited in electrochemical applications; however, ILs were quickly applied as solvents in several areas of chemistry, such as organic synthesis and catalysis [62]. They were also employed as lubricants [63], electrolytes for fuel cells [64] and solar cells [65], chromatography stationary phases [66], selective extraction [67] and enzyme supports [68].

3.2. Chemical synthesis of nanoparticles in ionic liquids

The potential of using ILs as solvents and stabilizing agents for NP synthesis was only recognized in the early 2000s. Pd [69] and Ir [70] nanoparticles were prepared by chemical reduction procedures, while Ge [71] NPs were produced via electrochemical methods. Just a few years later, TiO_2 [72] and CdSe [73] were prepared using ILs. Since those pioneering investigations, several kinds of nanostructures have been made using ILs. The vast majority of the studies have concentrated their efforts on the synthesis of metallic NPs and their catalytic applications. One very recent critical review of the topic covers the literature until 2010 [17].

Table 1
Examples of various metals sputtered onto silicon oil substrate.

Entry	Substrate	PVD conditions							Structure obtained		Ref.
		Method	Target	V (V)/i (mA)/P (W)	W_d (mm)	W_P (Pa)	D_T (s)	D_R (nm s^{-1})	S_T (°C)	Morphology	Size (nm)	
1	SO	RF-MS	Ag (99.99%)	–/–/50	80	0.2	510–570 s	0.8	RT	Irregular, thin Ag film	–	[44]
2	SO[a]	RF-MS	Al (99.95%) Ag (99.99%)	–/–/50	80	0.2	510–570 s	0.8	RT	Thin Al and Ag film with micrometer length scale	–	[43]
3	SO	RF-MS	Al (99.95%) Ag (99.99%)	–/–/50	60	0.2	420–600 s	–	18–120	Thin Al and Ag film with micrometer length scale	–	[45]
4	SO[b]	RF-MS	Ag (99.99%)	–/–/15, 30 and 50	60	0.2	120–240 s	0.4–1	17–100	Anomalous Ag film growth relaxation	–	[47]
5	SO	MS	Fe	5000/–/–	80	1–30	–	–	–	Spherical Fe and Ag NPs	9	[41]
			Ag	500/–/–							5–15	

V, voltage; i, current; P, power; W_d, work distance between target and liquid substrate surface; W_P, work pressure; D_T, deposition time; D_R, deposition rate; S_T, substrate temperature; RT, room temperature; SO, silicon oil; RF-MS, RF-magnetron sputtering; MS, magnetron sputtering; IL, ionic liquid.

[a] When the incident RF power was lower than 30 W, the Ag film could not be formed.

[b] To avoid the agglomeration of the particles, the surfactant sarcosyl oleic acid (Korantin from BASF AG) and a polyalkylene amine derivative (LP4 from ICI, Inc.) have been used. The surfactant (1 wt%) was dissolved in the carrier liquid before starting the sputtering process. In the absence of a surfactant, the sputtered Fe formed agglomerates of cubic particles with a mean diameter of 15 nm and a standard deviation of 1.2 nm.

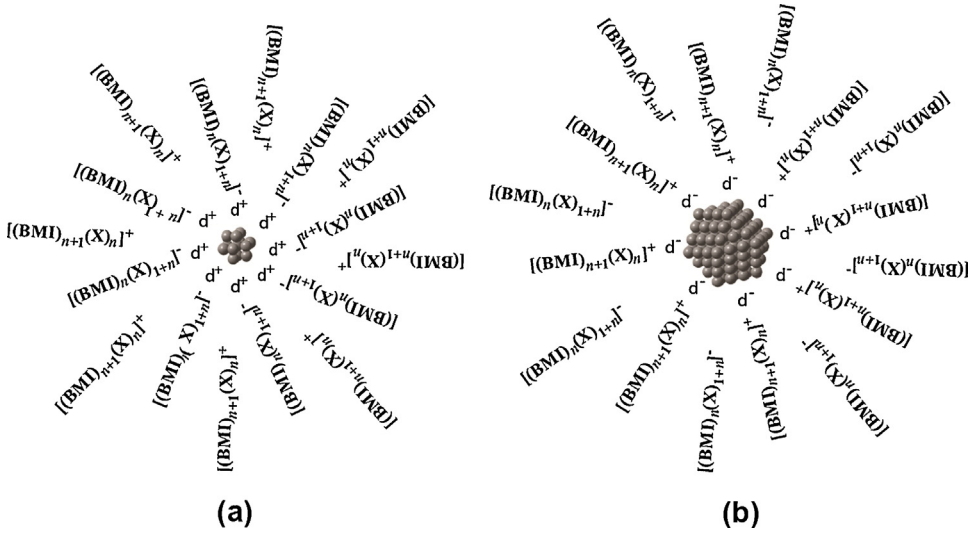

Fig. 3. Interaction of metal NPs with IL supramolecular aggregates: (a) small particles tend to interact preferentially with anionic aggregates of the ILs, whereas (b) large ones probably interact preferentially with the cationic aggregates [17].
Reprinted with permission from Ref. [17]. Copyright (2010) The Royal Society of Chemistry.

The interest in using ILs to synthesize nanostructures came from their peculiar physical–chemical properties. In addition to being very polar compounds, ILs can have low levels of interfacial tension. Because low interfacial tensions result in high nucleation rates, very small particles can be generated without suffering from Ostwald Ripening [74]. In other words, ILs easily change their molecular arrangements to adapt to NPs, providing a good stabilization for nanostructures. This adaptability is due to the hydrophobic and hydrophilic regions and high directional polarizability of ILs, enabling the molecules of the IL to become oriented parallel or perpendicular to the dissolved species [75]. Moreover, ILs have an unusual and outstanding property. They exhibit extended hydrogen bonding networks in the liquid state [76] and are therefore highly structured [77,78]. Thus, ILs can be considered to be supramolecular polymeric compounds with the composition $\{[(C)_x(X)_{x-n}]^{n+}[(C)_{x-n}(X)_x]^{n-}\}_m$, with C being the cation and X being the anion [79]. The property of supramolecular organization has enabled the use of ILs as entropic drivers [74] generating the concept of the IL effect [80]. Furthermore, due to their high thermal stability and low vapor pressure, there is no need to use high-pressure reactors in reactions with temperatures above 200 °C.

The way that the ILs control the growth of NPs produced by chemical procedures remains a topic of discussion in the literature. The most accepted mechanism of stabilization of NPs dispersed in non-functionalized ILs is the adsorption of anionic aggregates on the surface of the particles, which generates steric–coulombic stabilization [81]. Fig. 3 shows the proposed mechanism for a metallic nanoparticle stabilized with an IL derived from the 1-butyl-3-methylimidazolium (BMI) cation schematically.

The non-functionalized ILs provide steric/electronic stabilization of the "soluble" NPs by protective layers of discrete supramolecular $\{[(DAI)_x(X)_{x-n}]^{n+}[(DAI)_{x-n}(X)_x]^{n-}\}_m$ (where DAI is the dialkylimidazolium cation and X is the anion) species through the loosely-bound anionic and/or cationic and/or neutral moieties, non-polar imidazolium alkyl side chains and/or NHC species, together with an oxide layer (when present) on the metal surface [17]. The introduction of moieties on the imidazolium side chain, such as N^-, O^- and S^- containing groups may provide extra stabilization of the metal NPs through coordination with the metal surface.

Until now, the control of the size of the NPs in ILs was correlated with N-alkyl imidazolium side chains [82,83], anion volume [84,85] or anion coordination ability [86]. More recently, some studies have pointed out these same conclusions [80,87]. A number of authors have independently shown that the size of Ru and Ir nanoparticles is controlled by the nano-environment of the IL (hydrophobic or hydrophilic) in which the metal precursors are dissolved [88].

ILs have proven to be useful media for the synthesis of NPs. However, chemical synthesis has shown some critical problems. The poor solubility of the starting materials in the IL, the incompatibility of ILs with the majority of reducing agents, the incompatibility of ILs with alkaline species and the inability to remove ionic byproducts from the colloidal solutions restrict the applicability of nanoparticles in this medium. As mentioned earlier, ILs are suitable media for the synthesis of nanoparticles via sputtering methods. This approach overcomes all the problems of the chemical synthesis of nanoparticles in these fluids and opens up a new way to synthesize nanoparticles in an environmentally friendly way. Therefore, understanding the mechanism of nanoparticle growth via sputtering materials onto ILs and consequently the factors that control the shape and size of nanoparticles will lead to the design of new materials on the nanometric scale.

4. Sputtering deposition of nanoparticles onto ionic liquids

The sputtering deposition of nanoparticles onto ILs is a very new research area, which started in 2006 with the pioneering study of Kuwabata and co-authors [36]. Gold nanoparticles (Au NPs) about 5.5 nm in mean diameter and having a standard deviation of 0.9 nm were obtained after the sputtering of an Au target with Ar^+ ions directly onto the surface of the 1-ethyl-3-methylimidazolium tetrafluoroborate (EMI·BF_4) IL. When the experiments were done in a different IL, namely *N*,*N*,*N*-trimethyl-*N*-propylammonium bis(trifluoromethylsulfonyl)imide ($Me_3PrN{\cdot}NTf_2$), the Au NPs' mean size was 1.9 nm, with a standard deviation of 0.5 nm. The authors observed that the mean size of the particles formed depended on the IL used and not on the sputtering time, which only increased the concentration of Au NPs. The sputtering conditions applied were 4 mA of discharge current (discharge voltage not showed), 20 Pa of argon pressure, 5 min of sputtering time and a target–substrate distance of 35 mm. The importance of the discharge voltage will be discussed later.

The same research group published another study, showing the formation of gold–silver alloy nanoparticles in a single-step process by using a special target during sputtering deposition onto the 1-butyl-3-methylimidazolium hexafluorophosphate (BMI·PF_6) IL [89]. These bimetallic nanoparticles exhibited a compositional-sensitive surface plasmon resonance with a red-shifted peak, as the area of the gold increased on the targets. The sputtering conditions applied were 40 mA of deposition current (discharge voltage not showed), 5 min of sputtering time, 20 Pa of argon pressure and a target–substrate distance of 35 mm.

Following the same idea, Torimoto showed that the sputtering deposition of Ag on a BMI·PF_6 IL solution containing $HAuCl_4$ led to the formation of Au–Ag alloy nanoparticles through an in situ chemical reduction of Au via Ag deposition [90]. Moreover, it was exhibited that changing the discharge current from 10 to 40 mA increased the Ag nanoparticles' (prepared in pure BMI·PF_6) mean sizes from 5.7 to 11 nm, though increasing the sputtering time up to 50 min did not significantly change the size of the particles. It only increased the atomic concentration of Ag in the colloids [90]. The sputtering conditions were 10 mA of discharge current (discharge voltage missing) for 5 min at 5 Pa of argon pressure, with a target–substrate distance of 85 mm.

However, Nishikawa and co-workers, in collaboration with the previous cited team, published a contrasting result showing that the increase in the concentration of the sputtered metal caused an increase in the mean diameter of the particles formed, as shown by Small Angle X-ray Scattering (SAXS), Fig. 4a [91]. The effects of sputtering onto different alkyl chain lengths for BF_4^- anion-based ILs on particle size were also investigated. In this case, the size of the particles was correlated with the viscosity and surface tension of the ILs in the following manner: (i) the surface tension was important in the first step of the aggregation of Au atoms and/or small clusters that probably occurred on the liquid surface and (ii) the viscosity affected the dispersion of the nanoparticles formed onto the liquid phase. The sputtering conditions were 1 kV of discharge voltage, 5 mA of discharge current, 10–15 Pa of Ar pressure and 12–36 min of deposition. This was a very high discharge voltage, and it was maintained for a long time.

One year later, these authors realized that the apparent dependence of the nanoparticles' size on the Au concentrations, i.e., with sputtering time, was only due to the heating effects on the IL during the experiments. They discovered that controlling the substrate temperature and increasing the sputtering time did not cause the final particles' size to change. Moreover, increasing the substrate temperature from 20 to 80 °C for fixed sputtering conditions (1 kV, 20 mA, 12–13 Pa Ar pressure, 50 min of deposition and a target–substrate distance of 25 mm) resulted in an increase in both the nanoparticles' size and size distributions, Fig. 4b [92].

At the same time, our group observed that with an increase in the discharge current from 20 to 110 mA (and the voltage from 299 to 410 V) the mean size of the Au NPs prepared in the 1-*n*-butyl-3-methylimidazolium bis(trifluoromethylsulfonyl)amide (BMI·NTf_2) increased from 3.2 to 4.6 nm. With respect to the sputtering time, the nanoparticles' size did not change significantly when it was increased from 150 to 600 s [35]. Experiments were carried out at 40 mA (335 V), 2 Pa Ar pressure and a target–substrate distance of 50 mm. These results were in agreement with those of previous reports [90]. However, increasing the discharge current also caused the voltage to increase, and this cannot be factored out of the results. Further, we realized that the most important parameter governing NP size is probably the discharge voltage and not the current (to be discussed later). In addition, the effect of the IL anion was increased by fixing the cation BMI^+ associated with four different anions, i.e., bis(trifluoromethylsulfonyl)amide (NTf_2^-), hexafluorophosphate (PF_6^-), tetrafluoroborate (BF_4^-) and tri(pentafluoroethyl)trifluorophosphate (FAP^-). Fig. 5a–d shows

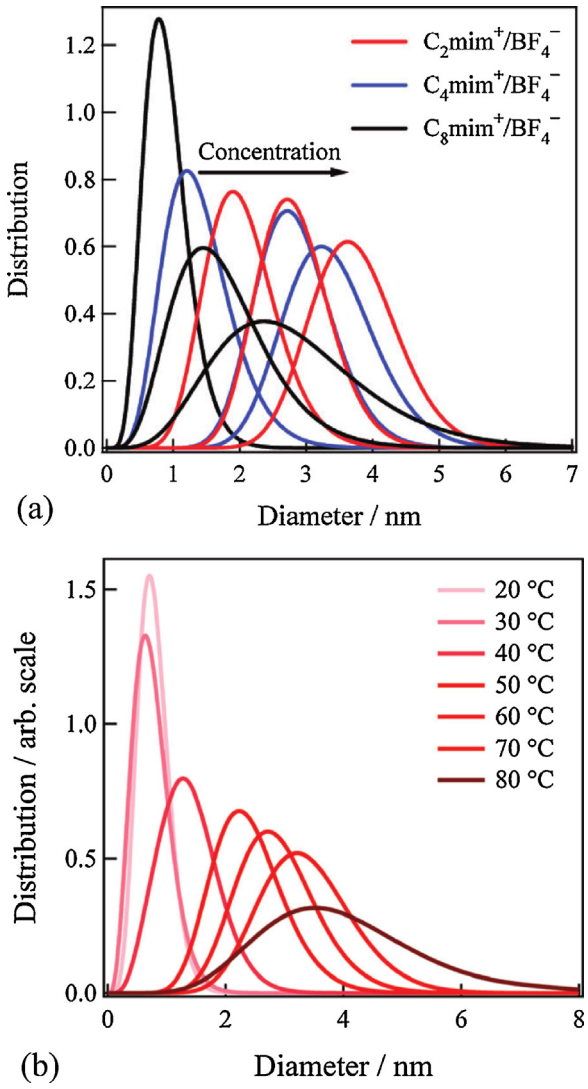

Fig. 4. (a) Particle size distributions of Au NPs generated (EMI·BF_4 (red), BMI·BF_4 (blue) and OMI·BF_4 (black)) by using various sputtering times. As the Au concentration increased, the size of the nanoparticles also increased [91]. (b) Particle-size distributions of Au NPs generated BMI·BF_4 at various temperatures [92].
Reprinted with permission from Ref. [91]. Copyright (2009) American Chemical Society. Reprinted with permission from Ref. [92]. Copyright (2010) American Chemical Society.

the Au NPs obtained after a sputtering deposition at 40 mA, 335 V, 300 s, 2 Pa Ar pressure and a target–substrate distance of 50 mm. According with the authors, the surface composition of the ILs seemed to be the most important parameter governing the size of the as-prepared Au NP's, especially with the increase in the fluorinated content, as in the case of BMI·FAP.

By using sputtering onto ILs, nanoparticles of various shapes and compositions could be prepared. For example, transition metal oxide nanoparticles that were highly dispersed onto ILs were prepared by sputtering W, Mo, Nb and Ti onto the EMI·BF_4. The particles' sizes were in the ranges of 3.2–4.8 for the W target, 2.7–3.7 for Mo, 1.9–2.9 for Nb and 3.4–4.6 for Ti. The particles' surface oxidized inside the ILs in a non-controlled way, with at least two oxide phases, as observed by XPS [93].

On the other hand, core–shell In-In_2O_3 nanoparticles were prepared by sputtering an In target onto four different BF_4^- anion-based ILs [94]. The size of the indium core was tunable from approximately 8 to 20 nm by using various alkyl side chain, whereas the shell thickness of the amorphous In_2O_3 was almost constant at

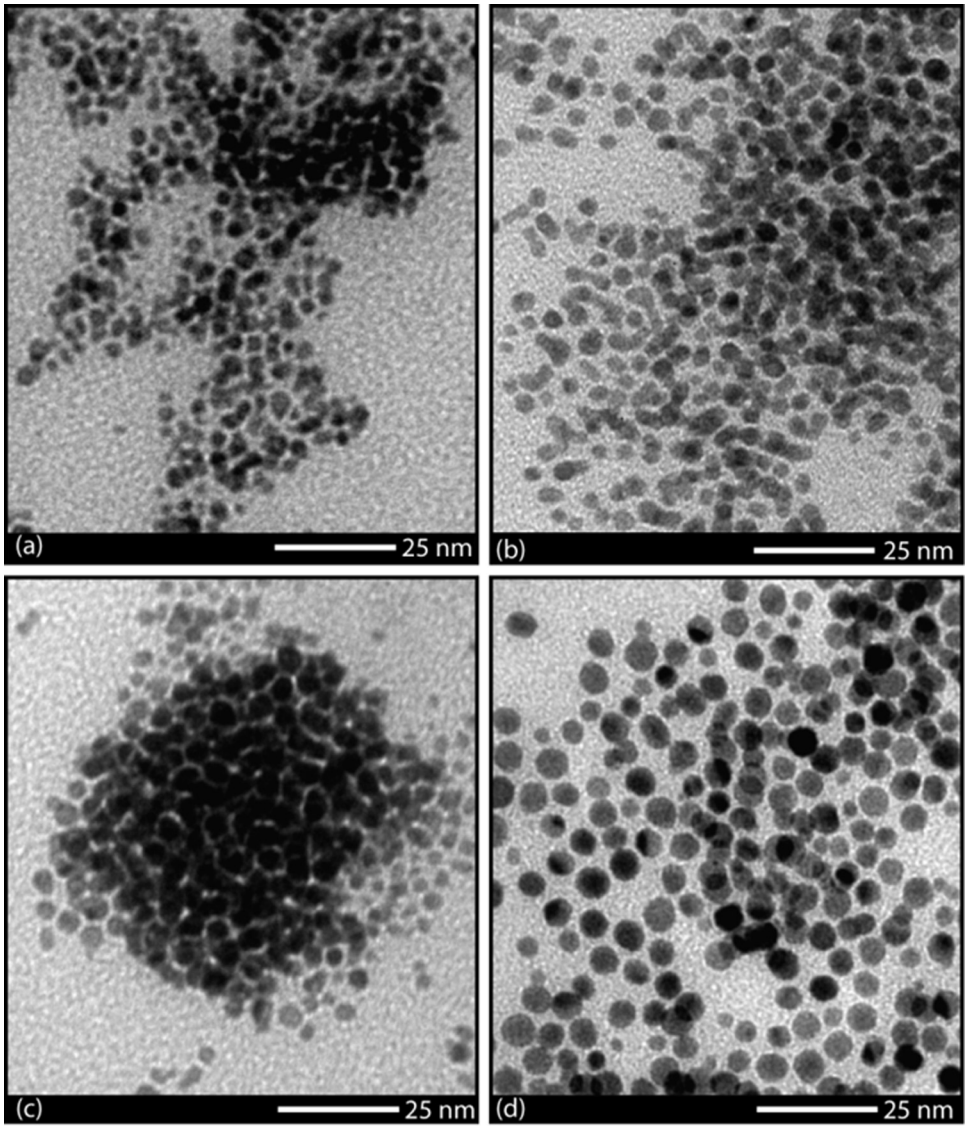

Fig. 5. TEM images of Au NPs sputtered onto ILs (a) BMI·NTf_2 (diameter 3.5 ± 0.6), (b) BMI·BF_4 (diameter 3.6 ± 0.4), (c) BMI·PF_6 (diameter 3.7 ± 0.4) and (d) BMI·FAP (diameter 4.9 ± 0.9) [35].
Reprinted with permission from Ref. [35]. Copyright (2010) American Chemical Society.

approximately 1.9 nm, as observed by TEM. Heat treatment of the thus-prepared particles at 523 K in air removed the core, resulting in the formation of hollow particles composed of crystalline In_2O_3, as illustrated in Fig. 6. The void of the hollow particles could be tuned from 4 to 10 nm during oxidation via selecting the size of the starting core–shell particles. The final size of the hollow particles was slight larger than that of the initial core–shell ones. The sputtering deposition in these studies was applied under the following conditions: 20 mA of current (discharge voltage missing), 2.0 Pa of argon pressure, 10 min of sputtering and a target–substrate distance of 20 mm.

Our group also prepared anisotropic gold nanodisks by direct sputtering onto a nitrile-functionalized IL [95]. The principal idea was the following: If the surface chemical composition of the liquid can control the initial formation of nanoparticles by sputtering [35], what will happens if we perform sputtering onto an IL with a functional group pointing out of its surface? Via the sputtering of an Au target onto 1-(butyronitrile)-3-methylimidazolium bis(trifluoromethylsulfonyl)imide (BCN)MI·NTf_2 IL with increased applied voltages, three phenomena were observed:

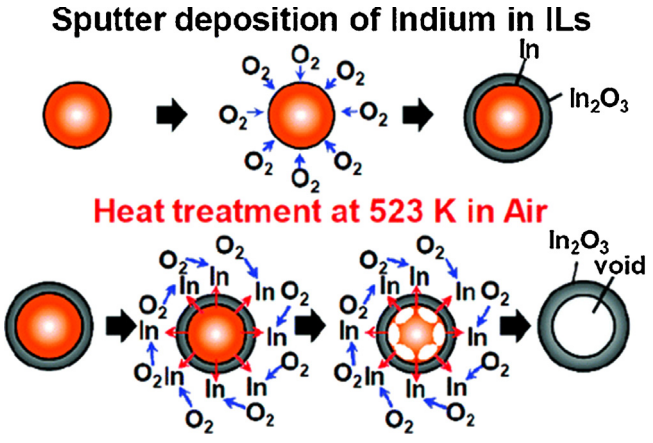

Fig. 6. Scheme showing the mechanism for core–shell In-In_2O_3 and void In_2O_3 NPs [94].
Reprinted with permission from Ref. [94]. Copyright (2010) American Chemical Society.

Table 2
SAXS fitting parameters (form, size and size distributions) of the colloidal Au NPs obtained via sputtering onto (BCN)MI·NTf_2 for 150 s at various discharge voltages [95].

Voltage (V)	Form factor	Diameter (nm)	Height (nm)	Standard deviation (%)
275	Sphere	4.0	4.0	33.0
	Ellipsoid	8.2	5.4	26.6
300	Sphere	6.2	6.2	6.0
	Ellipsoid	7.8	2.5	2.0
	Sphere	3.4	3.4	2.0
340	Sphere	6.6	6.6	17.6
	Ellipsoid	7.8	3.9	39.5
	Sphere	3.0	3.0	12
365	Sphere	9.6	9.6	105.4
	Sphere	5.4	5.4	52.2
410	Sphere	5.1	5.1	17.6

Reproduced by permission of the PCCP Owner Societies.

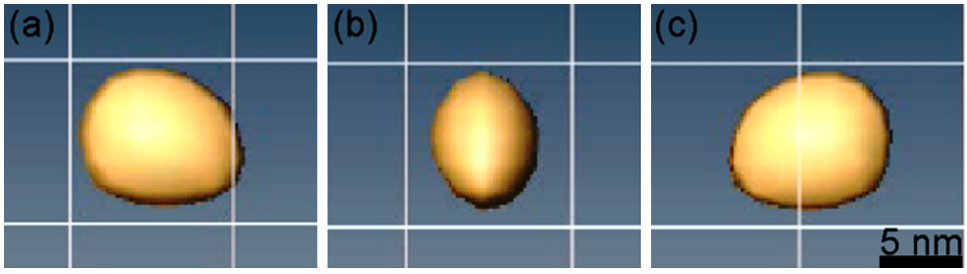

Fig. 7. TEM tomography images (video available at the original publication) of a selected Au nanodisk sputtered onto (BCN)MI·NTf_2 at a discharge voltage of 300 V for 150 s. From (a) to (c), the particle is gyrating to the left [95].
Reprinted with permission from Ref. [95]. Reproduced by permission of the PCCP Owner Societies.

(i) bimodal-sized distributions of Au nanospheres and Au nanodisks where obtained, and their sizes decreased; (ii) the population of particles with a lower diameter increased and (iii) the formation of anisotropic nanoparticles disappeared for voltages higher than 340 V [95]. Table 2 summarizes the presented results. The formation of the anisotropic particles was confirmed by TEM tomography (Fig. 7), SAXS and AFM analyses. The formation of anisotropic gold nanodisks was due to a strong interaction between sputtered Au atoms of low kinetic energies and the nitrile groups in the more external region of the IL surface. When the kinetic energy of the sputtered atoms was over a certain threshold, nanospheres were formed by Au–anion interactions in a slight internal region of the IL surface, as was observed for non-functionalized ILs [35]. This study showed the importance of the IL surface composition and also the sputtered atoms' kinetic energy in the process of the synthesis of nanoparticles via sputtering onto liquid surfaces.

However, recently, Binnemans and his research group published two important results concerning the formation of colloidal nanoparticles by this method. In the first one, the sputtering conditions were 50 mA of discharge current (discharge voltage missing), 10 Pa of Ar pressure, target–substrate distance of 40 mm, 4 mL of 1-butyl-3-methylimidazolium dicyanamide [BMI·$N(CN)_2$] IL and a deposition time of 60 s. Under these conditions, they founded that the IL changed from colorless to brown after the sputtering deposition of Au, and after some time, the colloid changed to a red color, as was expected for Au NPs larger than 2 nm [96]. These results were corroborated by UV–vis absorption spectroscopy and TEM. Immediately after the end of the sputtering process, only small particles in the range from 1 to 2.5 nm were observed, followed by the absence of the surface plasmon resonance (SPR) peak in the UV–vis spectrum. After 2 h, the same sample was analyzed again, and the population of 2 nm NPs was still predominant. Also, larger nanoparticles in the range from 3 to 7 nm were formed, along with the appearance of an SPR peak that increased in intensity as the elapsed time approached 24 h. This was due to the increase in the NP population in the size range of 3–7 nm, as viewed by TEM. The final NP size distribution was bimodal. The authors studied this growth for different ILs and found that it depended on the IL used. Based on the experimental data, the authors stated that the particles do not grow in the IL surface, as was reported earlier [35,36], but in the bulk liquid phase after the sputtering procedure via the aggregation of the smaller-sized nanoparticles formed during sputtering. The UV–vis results pointed out that the higher the viscosity of the liquids, the slower the growth kinetic of the particles.

In a second and more recent study, the Binnemans group also observed that, in addition to aggregation to form 5 to 6 nm Au NPs, two other processes were observed after sputtering, namely aggregation and sedimentation. The amount of water had a detrimental influence on the stability of the colloidal suspensions of the Au NPs in ILs [97].

Despite the ILs present very low vapor pressures compatible with ultra-high vacuum conditions and the properties needed to stabilize nanoparticles without using external reagents, they were not the only liquid substrates used for the sputtering of metal nanoparticles. For example, vegetable oils [42,98], liquid polyethylene glycol [99] and molten (6-mercaptohexyl)trimethylammonium bromide (6-MTAB) [100] were used to synthesis of metal nanoparticles. Table 3 summarizes some of the important results obtained in ILs to date.

5. Sputtering deposition onto vegetable oils

Vegetable oils are new, promising liquid substrates for sputtering deposition. The advantage of using vegetable oils is that they are abundant, inexpensive and biocompatible and also stabilize metallic NPs [42], as shown via chemical reduction [103]. In addition, the sputtering deposition does not require the addition of reducing agents to produce NPs, enabling less toxic nanostructures for

Table 3
Sputtering conditions of different materials onto ionic liquid substrates.

Entry	Substrate	Sputtering conditions								Structure obtained		Ref
		Method	Target	V (V)/i (mA)/P (W)	W_d (mm)	W_P (Pa)	D_T (min)	D_R (nm s^{-1})	S_T (°C)	Morphology	Size (nm)	
1	EMI·BF_4 Me_3PrN·NTf_2	MS	Au (99.99%)	–/4/–	35	20	5–120	–	–	Spherical Au NPs	5.5 ± 0.9 1.9 ± 0.5	[36]
2	BMI·PF_6 [a]	MS	Au (99.99%) and Ag (99.99%)	–/40/–	35	20	5	–	RT	Spherical Au NPs and bimetallic Au–Ag NP alloys	$Au_{100} = 2.6 \pm 0.3$ $Au_{75}Ag_{25} = 3.1 \pm 0.6$ $Au_{50}Ag_{50} = 6 \pm 1.5$ $Au_{25}Ag_{75} = 0.5$	[89]
3	EMI·BF_4 BMI·BF_4 OMI·BF_4	MS	Au (99.99%)	1000/5/–	25	10–15	12–36	–	–	Spherical Au NPs	0.75–3.5 nm, dependent on Au concentration and cation groups	[91]
4	Me_3PrN·NTf_2	MS	Au (99.99%)	–/40/–	35	20	5	–	–	Spherical Au NPs	2.3 ± 0.3	[101]
5	Me_3PrN·NTf_2	MS	Pt (99.98%)	–/40/–	–	7	5	–	RT	Spherical Pt NPs	Ar atm = 2.2 ± 0.4, N_2 atm = 3.3 ± 0.6, strongly dependent on gaseous species	[102]
6	BMI·BF_4	MS	Au (99.99%)	1000/20/–	25	12–13	50	–	20–80	Spherical Au NPs	0.6–3.5, strongly dependent on the temperature of the capture IL	[92]
8	BMI·NTf_2	MS	Au (99.99%)	299/20/6.1	50	2	2.5	0.20	RT	Spherical Au NPs	3.2 ± 0.5	[35]
				322/30/9.6			2.5	0.34			3.4 ± 0.5	
				335/40/13.4			2.5	0.42			3.5 ± 0.6	
				358/60/21.5			2.5	0.71			3.9 ± 0.8	
				410/110/45			2.5	1.65			4.6 ± 0.7	
				335/40/13.4			5	0.42			4.0 ± 0.9	
				335/40/13.4			7.5	0.42			3.9 ± 0.8	
				335/40/13.4			10	0.42			4.0 ± 0.8	
	BMI·BF_4			335/40/13.4			2.5	0.42			3.6 ± 0.4	
	BMI·PF_6			335/40/13.4			2.5	0.42			3.7 ± 0.4	
	BMI·FAP			335/40/13.4			2.5	0.42			4.9 ± 0.9	

V, voltage; i, current; P, power; W_d, work distance between target and liquid substrate surface; W_P, work pressure; D_T, deposition time; D_R, deposition rate; S_T, substrate temperature; RT, room temperature; MS, magnetron sputtering; IL, ionic liquid.

[a] The area fraction of gold foils on targets, f_{Au}, was defined as: $f_{Au} = A_{Au}/(A_{Au} + A_{Ag})$, where A_{Au} and A_{Ag} were total surface areas of gold and silver foils, respectively.

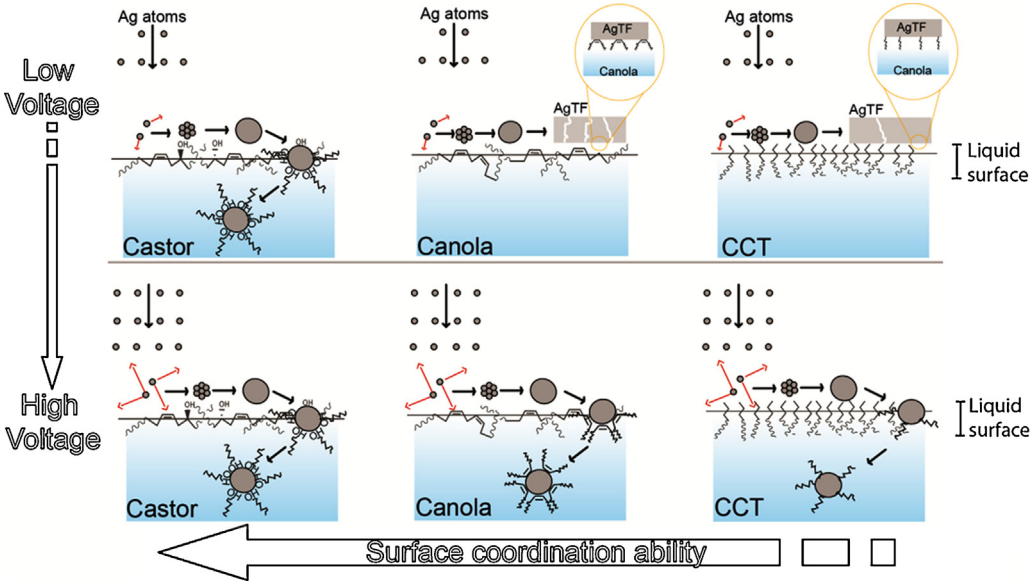

Fig. 8. Schematic illustration of the formation of Ag NPs or Ag TFs via the sputtering deposition of Ag onto different biocompatible liquids [98]. Reprinted with permission from Ref. [98]. Copyright (2011) American Chemical Society.

in vivo applications. Thus, this approach provides an easy, low-cost and fast synthesis of NPs, with potential applications within the fields of biology and medicine.

The sputtering of an Au target directly onto castor oil led to the formation of biocompatible Au NPs. The use of higher voltages during sputtering resulted in NPs of larger sizes, and higher sputtering times did not affect their mean sizes, as shown by TEM and SAXS [42].

An interesting point concerning the surface composition of vegetable oils and the applied voltage was recently discovered, and the formation of nanoparticles (first published in 1999) [41] or thin-films (first published in 1996) [44] by sputtering onto liquids was correlated with these parameters for the first time [98]. Wender and coworkers showed that the formation of NPs or thin-films depended on the applied voltages and the surface coordination ability of the different vegetable oils used. Lower discharge voltages and/or lower surface coordination abilities led to the formation of a film. Meanwhile, the opposite led to the formation of nanoparticles. Fig. 8 shows the scheme proposed. Higher discharge voltages mean higher diffusivities on the liquid surface (indicated by the red arrows), facilitating the penetration and/or attachment of the atoms/nucleus to the functional groups of the liquid surface. For the liquids studied, nanoparticles were easily formed in castor oil, which has a hydroxyl group, in almost all sputtering conditions, while in canola oil, which is predominantly composed of unsaturated aliphatic chains, and in caprylic/capric triglyceride (CCT, composed solely of saturated alkyl chains) thin films were formed at low voltages and NPs were formed at high discharge voltages. The lower the oil surface coordination ability, the higher the discharge voltage necessary to form colloidal nanoparticles.

6. Mechanisms of nanoparticles formation: present discussions

As the reader can see, the results published to date are contradictory [35,36,91,92,95–98]. It seems to be the consensus that the nature of the liquids used plays a predominant role controlling nanoparticle formation. However, the current discussion in the scientific literature is related to where and how the liquids control the growth of the NPs. Some groups point out that the surface and/or bulk liquid composition governs the mechanism [35,42,98,104], and others point out that the liquid viscosity and surface tension control the growth process [36,91,92,94,97,99]. Moreover, there are several parameters that can influence the formation of nanoparticles via sputtering. Unfortunately, little attention was paid to these factors in the first reports, and some authors did not properly describe all the parameters used for the sputtering, making any reasonable comparison between the results impossible. Also, the conditions applied were very different, and the results cannot be correlated, because the formation mechanism can be sensitive to the parameters, as with, for example, the discharge voltage [98].

Wender et al. [35] provided some insights into the mechanism of NP growth via sputtering onto liquids by postulating three different scenarios: (i) the atomic nucleation starts on the IL surface and then diffuses into the liquid phase, where particle growth takes place; (ii) both processes occur on the IL surface or (iii) the metal atoms and clusters penetrate to just below the liquid surface, and both processes occur in the bulk IL phase (Fig. 9i–iii).

Actually, the environment in which the metal NPs are formed must be dependent on how deeply the sputtered atoms can enter in bulk liquid phase. In other words, the extent of the penetration of the atoms is a function of their kinetic energy. Thus, the sputtering conditions (voltage, inert gas pressure, target temperature and liquid–target distance) must influence the NP size distribution. Moreover, how the properties of the liquid environment (surface or bulk) control the growth kinetics is still a topic of discussion. Inasmuch, secondary growth can occur during colloid aging or temperature increase [92,97].

Nishikawa's group published a recent study in which conditions such as sputtering discharge current, discharge voltage, target–substrate distance, sputtering time and target temperature were investigated. They concluded that the temperature of the target and the applied voltages have a strong influence on the size of the Au NPs generated via sputtering onto BMI·BF_4 IL, while the target–substrate distance, sputtering time, argon pressure and discharge current have little or no influence [105]. They stated that for the generation of smaller particles, low liquid and target temperatures and high applied voltages are desirable. Wender et al. [42,98] had previously described the discharge voltage as governing the size of sputtered nanoparticles. It is well-known that the discharge voltage is related to the energy of the sputtered atoms, which will

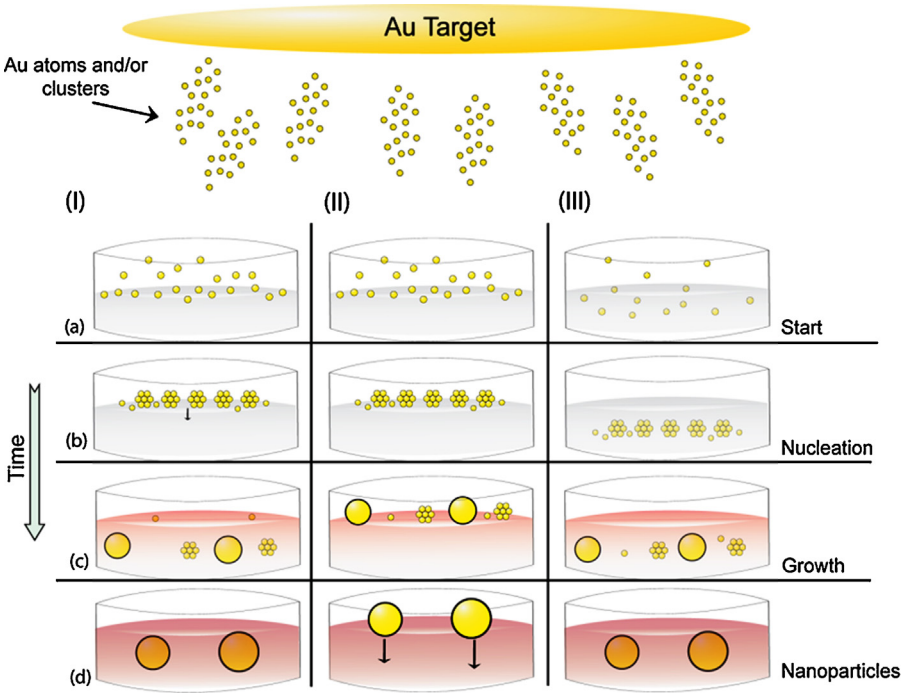

Fig. 9. Possible mechanisms for the nucleation and growth of sputtered gold nanoparticles into ILs [35]. Reprinted with permission from Ref. [35]. Copyright (2010) American Chemical Society.

depend on the inert gas and target used and are in a range of a few eV. However, the discharge voltage's effect on NP size is not yet well understood. At the same time that the NP size increased with the discharge voltage for sputtering Au or Ag onto castor oil [42,98], it decreased for two ILs, namely (BCN)MI·NTf_2 and BMI·BF_4 [98,105]. Therefore, the discharge voltage dependence seems to be more complicated and to correlate not only with the liquid used but also with the sputtering conditions and target properties. Moreover, Wender et al. have shown that for the same liquid substrate, higher voltages led to nanoparticle formation. Meanwhile, lower voltages resulted in the formation of a thin-film on the top surface of the liquid [98].

Another intensively studied parameter was the discharge current, which is directly related with the number of atoms ejected from the target per second, i.e., the sputtering rate. Torimoto and coworkers showed that the size of Ag NPs increased with increased discharge current for Ag deposition onto BMI·PF_6 (target located 85 mm from the liquid surface of 10 cm^2 area, deposition of 5 min at 5 Pa of Ar, and discharge voltage not shown) [90]. Our group also reported such behavior when depositing Au onto BMI·NTf_2. However, we further realized that the principal effect was the discharge voltage and not the current [98]. Nishikawa recently commented on the two cases presented herein after not finding any significant variations in NP size for Au sputtered onto BMI·BF_4 at 700 and 1000 V for various discharge currents [105]. They believe that in the previous cases [35,90], the particle size increased due to the heating of the liquid surface when the current was increased. They utilized high discharge voltages (near 1 kV), and further investigation is still needed to determine its importance in nanoparticle formation. Our group focused in performing sputtering over short times (from 1 to 5 min) and low discharge voltages (from 280 to 465 V). By measuring the IL's surface temperatures immediately after venting the deposition chamber (less than 2 min) only small variations of about 1 °C could be detected by using a thermocouple of 0.1 °C sensitivity. Therefore, we do not believe in the existence of temperature effects in the conditions we studied. On the other hand, some groups performed deposition for too long a time, and in these cases, temperature effects were decisive [91,92]. By controlling the IL surface temperature, they showed that it strongly affects nanoparticle formation [92].

According to recent reports, the effect of IL surface tension itself should be discarded, as was proposed initially [36], because heating linearly diminished the surface tension of the BMI·BF_4 from 43.5 to 40.2 mJ m^{-2} and consequently the time that the particles would stay in the liquid surface to grow [92]. If it was important, the result would have been exactly the contrary, i.e., there would have been a decrease in the final size and not an increase, as was observed. Finally, the authors interpreted their results in terms of the viscosity of the ILs, considering the particles aggregating inside the liquid phase [92].

A number of authors considered that the surface tension and the viscosity of the liquids might be controlling the growth of the nanoparticles. However, our group argues that the liquid surface composition and coordination ability play major roles in the nanoparticle formation, instead of viscosity or surface tension, which sufficiently explains some of the literature results obtained to date [98]. Moreover, if the growth of NPs occurred in the IL bulk, an increase in Au NP size with an increase of anion volume would be expected [35,80,84,85]. This was not observed and it was pointed out that both nucleation and nanoparticle growth seem to occur at the IL surface, as in case (ii) of Fig. 9. This shows the importance of the chemistry of surface functional groups at the IL/vacuum interfaces [98]. In addition, the difference in size could not be correlated with the macroscopic properties of the ILs, such as surface tension and viscosity [35].

In addition, Binnemans and coworkers are the only researchers who show the growth of the nanoparticles after sputtering, i.e., as a second step [96,97]. However, they performed the sputtering over very short time periods (~60 s) onto high IL volumes (~4 mL). In this case, the Au concentration is considerably different from the other cases presented [35,36,91]. Even though these results open up new discussions about the initial mechanisms of NP formation, some care should be taken in the future studies. Probably, the sputtered atoms arise at the liquid surface, diffuse to the liquid bulk after

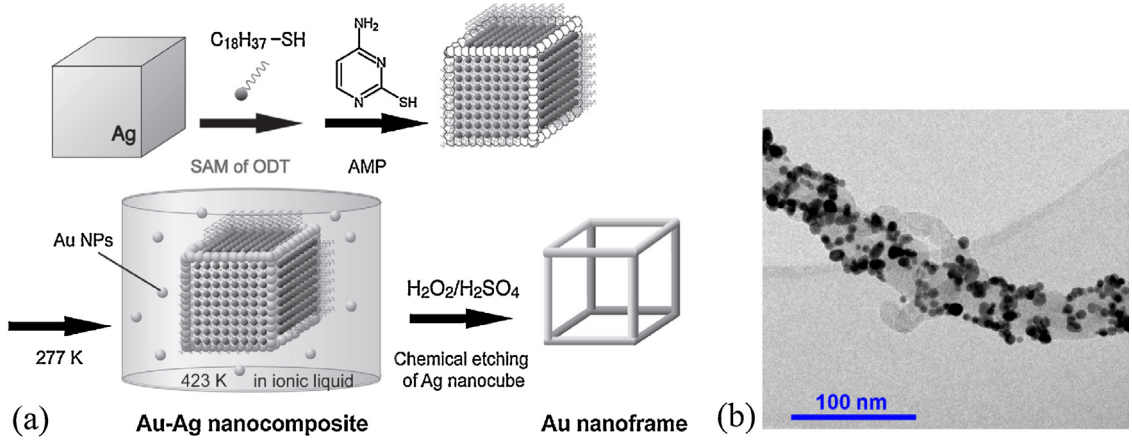

Fig. 10. (a) Illustration of the procedure to place the Au nanoframe onto Ag nanocubes in IL [111] and (b) TEM image of metallic NPs dispersed on a carbon structure [112]. Reprinted with permission from Ref. [111]. Copyright (2011) Chemical Society of Japan. Reprinted with permission from Ref. [112]. Copyright (2012) Elsevier Ltd.

the nucleation processes, and then start to grow. This can explain both the nanoparticle and thin-film formation. However, it will strongly and synergistically depend on the sputtering conditions and on the liquid properties. In other words, for one case, under specific sputtering condition, the nanoparticles could grow on the liquid surface, resulting in the formation of anisotropic nanoparticles [98] or thin-films [59,98], and in other cases, they could grow on the bulk liquid phase [91,96,105]. Despite the confusing data presented to date, the knowledge regarding this synthesis technique is increasing exponentially as the years pass.

Therefore, it is believed that to obtain deeper insight regarding the mechanism of nanoparticle formation, the key issue will be to develop in situ experiments in order to investigate nanoparticle formation from the first seconds of deposition until complete formation and possibly the agglomeration of the nanoparticles. Also, future experiments should be carried out carefully with respect to sputtering conditions, i.e., discharge current, discharge voltage, deposition pressure, target–substrate distance, deposition time, substrate temperature, target temperature, etc.

7. Applications

As shown above, sputtering can be considered an important and innovative approach to producing soluble and stable NPs in low-vapor-pressure liquid substrates. The easy and fast synthesis that is allied to this green method can be considered to be the major differential of this route to potential applications. Over time periods ranging from a few seconds to a few minutes, stable colloidal NPs can be produced without any chemical stabilizing and/or reducing agents. Therefore, sputtering is a useful method for the preparation of ultrapure NPs or thin films on liquid or solid substrates.

These characteristics and virtues open new lines of applications that until now, had been complicated by the high cost of production and/or the difficulty of obtaining a suitable final product. Here, some applications that arise from this new technology will be presented.

7.1. Nanoparticles dispersed on a solid surface

The dispersion of sputtered NPs onto a solid surface was demonstrated by Torimoto et al. [106]. They showed that the adsorption of Au NPs on a TiO_2 (1 1 1) substrate varied with the IL that was encapsulating the NPs on the TiO_2 surface. A strategy was proposed in order to control the positions of the Au NPs on the solid substrates via the electrostatic interaction between the ILs' thin layers on the substrate surface, in addition to non-covalent interactions between the ILs. The microscopic charge array of the Ti^{4+} and O^{2-} ions on the surface can work to order the NPs and ILs. Subsequent treatments immobilized the NPs and removed the IL layers, resulting in Au NP's self-assembled arrays on TiO_2 (1 1 0) substrate.

Moreover, metal nanoparticles have also been obtained using "non" conventional sputtering chambers. For example, a new method was reported to form metal nanoparticles by sputter deposition inside a reactive ion-etching chamber with a very short target–substrate distance. The size distribution and morphology of nanoparticles are influenced by the distance, the ion concentration, and the sputtering time [107]. Passivated gold nanoparticles were synthesized through a microwave-assisted process in a two-phase system, in the presence of 1-dodecanethiol and these nanoparticles spontaneously self-assemble into self-supported superstructures [108]. The controlled synthesis of bismuth nanoparticles can be achieved by vapor condensation in tube flows [109]. A new sputtering chamber containing an electromagnetic oscillator (with variable controlled frequency) that allowed the constant movement of the conical flask, which contains the support has been recently reported. This new chamber allows the production of magnetic biocatalysts, by simple sputtering of Ni nanoparticles onto enzyme surfaces. This new technique provided high levels of recovery, reusability and catalytic activity for the lipase-Ni biocatalysts [110].

7.2. Nanoparticle immobilization onto inorganic structures dispersed in ILs

Two strategies were used to immobilize NPs onto inorganic structures dispersed in ILs. In the first study, the Au NPs prepared via sputtering deposition in an IL were selectively assembled at the edges and vertices of Ag nanocubes, the surfaces of which were modified with a self-assembled monolayer of 1-octadecanethiol and 4-amino-2-mercaptopyrimidine. After a specific chemical etching of Ag, the sample resulted in Au–Ag binary nanocomposite and Au nanoframe formation (see scheme in Fig. 10a) [111]. The second strategy consisted of depositing small metallic NPs, such as Au, Ag, Pd [112] and Pt [113], which were produced by sputtering onto the ILs, on diverse carbon nanostructures dispersed in a room-temperature IL. The size of the metal nanoparticles could be controlled by the composition of room-temperature ILs, and the surface density of the metal nanoparticles could be controlled via the sputtering conditions. Fig. 10b shows a metal NP self-assembled on carbon. The self-assembled structure is driven by the interlinking interactions among the metal nanoparticles, IL cations, and carbon nanostructures.

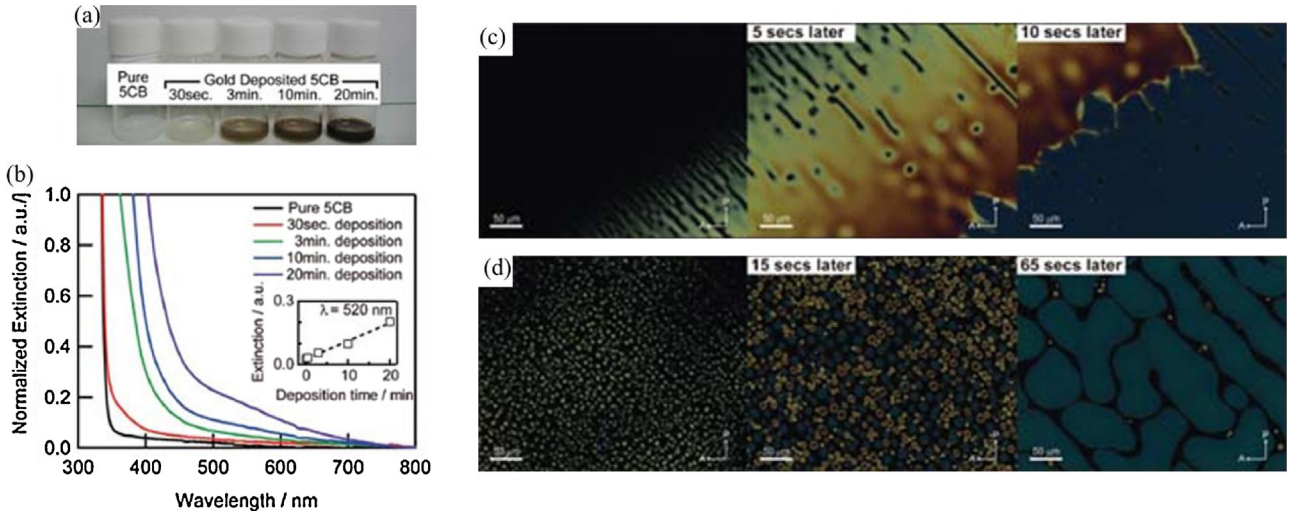

Fig. 11. (a) Photograph and (b) extinction spectra of nematic LC 5CB gold deposited for various sputtering times. (c) Phase transition behavior of the pure 5CB at 35.4 °C, where the appearance of the nematic phase is observed as a "front" that passes through the field of view. (d) Phase transition behavior of the NPs dispersed onto 5CB at 32.6 °C, where the small bubble-like domains of the nematic phase appear and gradually grow to fill the sample [114].
Reprinted with permission from Ref. [114]. Copyright (2010) WILEY-VCH Verlag GmbH & Co. KGaA, Weinheim.

7.3. Nanoparticle dispersed liquid crystals

Ozaki and coworkers [114] demonstrated a method that can drastically simplify the procedure used to fabricate metal NP–liquid crystal (LC) suspensions. Such suspensions can be fabricated via sputter depositing the target material onto the host LC. Certain LC molecules also possess a vapor pressure that is smaller than 1 Pa at room temperature, which is sufficient for them to undergo the sputtering deposition process. Fig. 11a shows the photographs of 4-pentyl-4′-cyanobiphenyl (5CB), a compound with a nematic phase between 24 and 35 °C, before and after the sputtering deposition of gold. The extinction spectrum of the material shown in Fig. 11b reveals that the coloring of the LC is, in fact, attributed to the local surface plasmon resonance of gold, which is observed as a slight shoulder at around 520 nm. To observe the NPs on the LC, standard polarization optical microscopy was performed on the sample, which was placed in a planar rubbed sandwich cell to investigate whether the sample was free from aggregations in the conventional LC device geometries, see Fig. 11c and d.

7.4. Catalysis

One of the main applications of metallic NPs produced via sputtering onto ILs is in the field of catalysis. Although few examples have been reported, the results obtained are interesting. Most of the studies in the literature are focused on the electrocatalytic activity of metallic NPs for the O_2 reduction reaction (ORR), which is an important reaction for fuel cell applications.

The majority of the papers reported the use of Pt NPs supported on carbonaceous supports for the ORR [102], except for one example that applied Au NPs deposited over High-Oriented Pyrolytic Graphite (HOPG) as an electrocatalyst [101]. The NPs were produced via the sputtering of a metallic target over the IL and then immobilized onto the support by heating a mixture of carbon and the IL/NPs at various temperatures. The IL was removed via solvent extraction after the immobilization. The thermal treatment conditions influenced the size and amount of NPs retained onto the electrode surface [101,102]. For example, Au NPs were deposited over HOPG from the IL $Me_3PrN{\cdot}NTf_2$ and $BMI{\cdot}PF_6$ at room temperature (RT), 373 K and 423 K [101]. TEM analysis of the electrodes prepared at room temperature showed only a few Au NPs in an island-like morphology, with a mean height equal to the initial NPs diameter, 2.3 nm. As the temperature increased, greater numbers of nanoparticles could be observed, and the surface of the HOPG was almost fully covered by Au NPs. Moreover, the height (measured by AFM) of the nanoparticles also increased. The mean heights obtained were 5.4 nm and 10 nm at 373 and 423 K, respectively. The hydrophobic nature of the IL also influenced the number of NPs deposited onto the surface of the electrode. The more hydrophobic anion, NTf_2, favored the deposition of Au NPs over the HOPG, while the PF_6 anion allowed the deposition of sparsely aggregated NPs, even after thermal treatment. The obtained Au NPs/HOPG showed a reversible two-electron reduction of O_2 to HO^{2-} in an O_2-saturated 0.5 mol dm^{-3} aqueous KOH solution, which was typical of Au (1 1 1) and Au (1 1 0) surface-enriched particles [101].

The properties of the Pt NPs deposited onto Glassy Carbon (GC) also showed the important influence of the heating process. The size of the Pt NPs increased with the thermal treatment, changing from 2.2 nm, as they were prepared, to a maximum diameter of 3.7 nm above 423 K [115]. Moreover, heating temperature is also a fundamental parameter for the ORR using O_2-saturated 0.5 mol L^{-1} H_2SO_4 solutions. The Pt/GC electrodes obtained only showed ORR currents when heated to temperatures above 423 K [102]. Additionally, the Pt/GC showed a maximum activity when treated at 473 K, as shown in Fig. 12.

Another catalytic application for the NPs produced via sputtering onto ILs is the Suzuki–Miyaura reaction, which is catalyzed by Pd NPs [116]. Miura and co-workers have applied Pd NPs formed in the ILs $BMI{\cdot}PF_6$ and $BMI{\cdot}NTf_2$ to the cross-coupling reaction between various Aryl iodides and bromides with arylboronic acids. The catalytic reactions were optimized for two IL/nanoparticle suspensions under biphasic conditions by using 0.2% Pd, water as a solvent and various bases. The best base to use with $BMI{\cdot}PF_6$ was di-isopropylethylamine (DIPEA). With $BMI{\cdot}NTf_2$, the best base is Cs_2CO_3 at 80 °C.

7.5. Miscellaneous applications

The synthesis of NPs by the sputtering of metal targets onto ILs is a relatively new topic. Thus, few applications for these materials have been reported to date. In this sub-section, two kinds of application found in the literature will be shown.

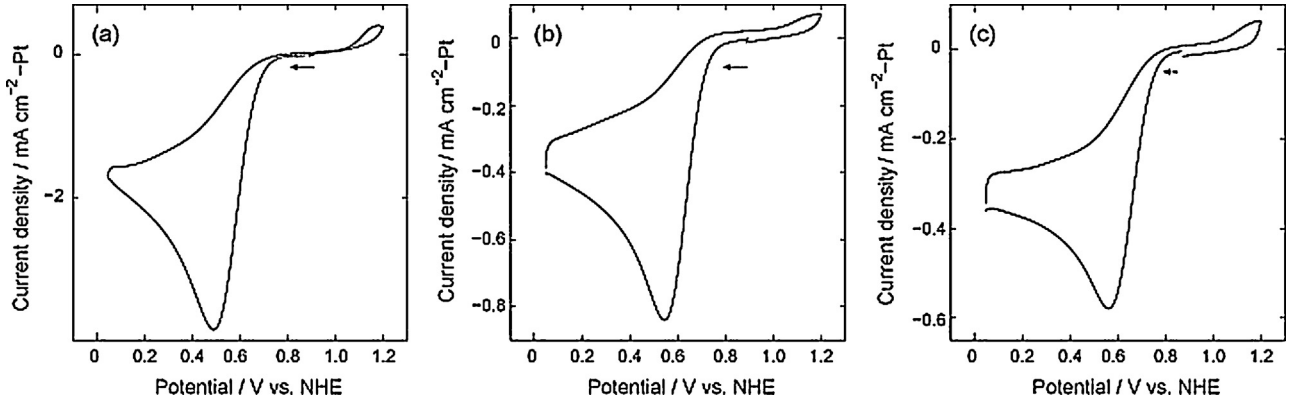

Fig. 12. Cyclic voltammograms recorded at Pt-GCEs in O_2-saturated 0.5 M H_2SO_4 aqueous solution at 298 K. The temperatures for the Pt-GCE preparation were (a) 473 K, (b) 523 K and (c) 573 K. The scan rate was 10 mV s^{-1} [115].
Reprinted with permission from Ref. [115]. Copyright (2010) Elsevier Ltd.

The first one is the use of Au NPs for plasmonic devices. Torimoto et al. have produced Au NP layers over quartz that enhanced the photoluminescence (PL) of CdTe nanocrystals [117]. The samples studied were produced by heating an imidazolium surface-modified quartz slide with Au NPs/BMI·PF_6 colloids produced via sputtering. The Au layer was then covered with polyelectrolyte bi-layers of various thicknesses, on which a layer of thioglycolic acid-capped CdTe NPs were adsorbed. The PL enhancement was increased via the Au NPs, and this augmentation was strongly dependent on the distance between the semiconductor nanoparticles and the Au layer, which became higher as the number of polyelectrolyte layers deposited on the plasmonic NPs increased.

The second application is the use of Ag NPs produced via sputtering as a sacrificial Ag^+ reservoir for antimicrobial composite coatings [118]. Glass substrates were coated with a SiO_2/IL/Ag NP nanocomposite that was produced by using sol-gel, and its antimicrobial activity was evaluated against *Pseudomonas aeruginosa* bacteria. The bactericidal activity of the coatings was due to the synergetic combination of all the components of the composite and was strongly dependent on the type of IL used. For example, the Ag NPs produced in EMI·NTf_2 showed a poor level of activity against the bacteria used, while the methyltrioctylammonium bis(trifluoromethylsulfonyl)imide (N_{8881}·NTf_2) annihilated the microorganisms almost completely, as shown in Fig. 13.

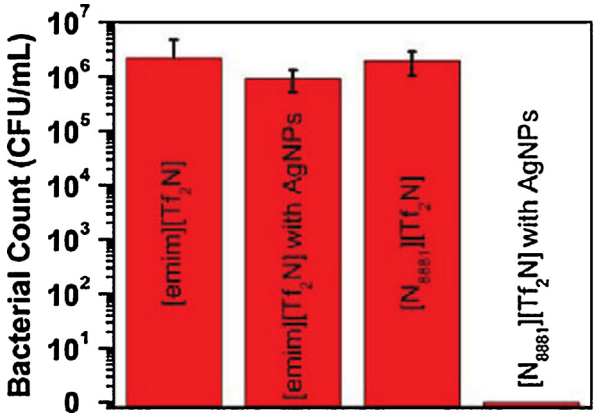

Fig. 13. Antimicrobial activity of sol–gel nanocomposite films with two ILs. (9.3 wt%, incubation time: 24 h) [118].
Reprinted with permission from Ref. [118]. Copyright (2012) American Chemical Society.

8. Conclusions and future trends

Without doubt, the sputtering deposition of metals onto liquids represents a new, efficient and simple method via which to synthesize stable colloidal NPs in ILs and vegetable oils. This physical process (sputtering) eliminates chemical residuals during NP synthesis because no stabilizing or reducing agent is used. Sputtering onto liquid substrates is a very versatile way to prepare metallic, magnetic and semiconductor NPs. Instead of a simple deposition, this technique can be performed with the co-evaporation of various targets on the surface of the liquid, resulting in a specific composition of nanostructures.

The physical parameters used during sputtering could allow for the prompt control of NP size, size distribution and concentration. Some results have suggested that NP growth occurs on the IL surface and that the composition at the liquid/vacuum interface [119] determines the size and size distribution of the Au NPs. In the case of castor oil, a threshold voltage has been found for the mechanism of NP formation due to the environment the nucleation takes place in.

However, the IL surface properties, ion orientation and chemical composition are not yet fully understood with regard to sputtering. Future investigations must be carried out in order to discover the mechanisms of NP growth. The materials produced via this technique are very pure and can improve the properties of the final products.

To conclude, due to the aforementioned properties, industrial availability and low cost, the sputtering method is one of the most promising in the field of nanomaterial colloidal synthesis for a variety of applications. The possibility of synthesizing metallic, bimetallic, semiconductor and magnetic nanoparticles is one of the advantages of this technique. Moreover, sputtering is a controllable and stable process that can be used to prepare small-sized (1–10 nm) colloidal nanoparticles. The target composition can be specially manipulated, or chemical-reducing processes can be initiated during sputtering in order to prepare colloidal bimetallic or semiconductor nanoparticles, such as PbSe and CdTe, for various applications. Moreover, as a simple deposition, sputtering can be performed via the co-evaporation of various targets onto the surface of the IL, resulting in nanostructures with the desired composition.

However, ILs and silicon oil are not fully environmentally friendly or biocompatible with the preparation of NPs for biological, pharmaceutical or medical applications. In this respect, vegetable oils open up new possibilities for the synthesis of a variety of biocompatible nanomaterials with applications, for example, in cancer

therapy and drug delivery [42]. Therefore, the formation mechanisms of the NPs via sputtering atoms onto the surfaces of liquids are not yet totally understood, and future investigation is necessary in order to fully understand the entire process.

Acknowledgments

Thanks are due to the following agencies for financial support: CNPq, CAPES, FAPERGS, TWAS, the Humboldt Foundation, INCT-Catal., MCT, FAPESP under Project 2011/17402-9 and PETROBRAS.

References

[1] C. Burda, X.B. Chen, R. Narayanan, M.A. El-Sayed, Chem. Rev. 105 (2005) 1025.
[2] L. Armelao, D. Barreca, G. Bottaro, A. Gasparotto, S. Gross, C. Maragno, E. Tondello, Coord. Chem. Rev. 250 (2006) 1294.
[3] M.C. Daniel, D. Astruc, Chem. Rev. 104 (2004) 293.
[4] Y.G. Sun, Y.N. Xia, Science 298 (2002) 2176.
[5] J.H. Li, J.Z. Zhang, Coord. Chem. Rev. 253 (2009) 3015.
[6] K.L. Kelly, E. Coronado, L.L. Zhao, G.C. Schatz, J. Phys. Chem. B 107 (2003) 668.
[7] W.L. Barnes, A. Dereux, T.W. Ebbesen, Nature 424 (2003) 824.
[8] L. Armelao, S. Quici, F. Barigelletti, G. Accorsi, G. Bottaro, M. Cavazzini, E. Tondello, Coord. Chem. Rev. 254 (2010) 487.
[9] F. Wang, X.G. Liu, Chem. Soc. Rev. 38 (2009) 976.
[10] U. Resch-Genger, M. Grabolle, S. Cavaliere-Jaricot, R. Nitschke, T. Nann, Nat. Methods 5 (2008) 763.
[11] T. Trindade, P. O'Brien, N.L. Pickett, Chem. Mater. 13 (2001) 3843.
[12] D.M. Adams, L. Brus, C.E.D. Chidsey, S. Creager, C. Creutz, C.R. Kagan, P.V. Kamat, M. Lieberman, S. Lindsay, R.A. Marcus, R.M. Metzger, M.E. Michel-Beyerle, J.R. Miller, M.D. Newton, D.R. Rolison, O. Sankey, K.S. Schanze, J. Yardley, X.Y. Zhu, J. Phys. Chem. B 107 (2003) 6668.
[13] P. Poizot, S. Laruelle, S. Grugeon, L. Dupont, J.M. Tarascon, Nature 407 (2000) 496.
[14] A. Bezryadin, C. Dekker, G. Schmid, Appl. Phys. Lett. 71 (1997) 1273.
[15] R.M. Crooks, M.Q. Zhao, L. Sun, V. Chechik, L.K. Yeung, Acc. Chem. Res. 34 (2001) 181.
[16] S.H. Joo, S.J. Choi, I. Oh, J. Kwak, Z. Liu, O. Terasaki, R. Ryoo, Nature 412 (2001) 169.
[17] J. Dupont, J.D. Scholten, Chem. Soc. Rev. 39 (2010) 1780.
[18] J.D. Scholten, B.C. Leal, J. Dupont, ACS Catal. 2 (2012) 184.
[19] A.M. Trzeciak, J.J. Ziolkowski, Coord. Chem. Rev. 251 (2007) 1281.
[20] N. Yan, C.X. Xiao, Y. Kou, Coord. Chem. Rev. 254 (2010) 1179.
[21] V. Subramanian, E. Wolf, P.V. Kamat, J. Phys. Chem. B 105 (2001) 11439.
[22] T. Hasobe, H. Imahori, P.V. Kamat, T.K. Ahn, S.K. Kim, D. Kim, A. Fujimoto, T. Hirakawa, S. Fukuzumi, J. Am. Chem. Soc. 127 (2005) 1216.
[23] A. Kongkanand, K. Tvrdy, K. Takechi, M. Kuno, P.V. Kamat, J. Am. Chem. Soc. 130 (2008) 4007.
[24] M. Bruchez, M. Moronne, P. Gin, S. Weiss, A.P. Alivisatos, Science 281 (1998) 2013.
[25] Q.A. Pankhurst, J. Connolly, S.K. Jones, J. Dobson, J. Phys. D: Appl. Phys. 36 (2003) R167.
[26] X.H. Gao, Y.Y. Cui, R.M. Levenson, L.W.K. Chung, S.M. Nie, Nat. Biotechnol. 22 (2004) 969.
[27] N.L. Rosi, C.A. Mirkin, Chem. Rev. 105 (2005) 1547.
[28] Y.F. Hao, G.W. Meng, C.H. Ye, L.D. Zhang, Cryst. Growth Des. 5 (2005) 1617.
[29] M. Okumura, S. Tsubota, M. Iwamoto, M. Haruta, Chem. Lett. (1998) 315.
[30] A. Reina, X.T. Jia, J. Ho, D. Nezich, H.B. Son, V. Bulovic, M.S. Dresselhaus, J. Kong, Nano Lett. 9 (2009) 30.
[31] K. Sivula, F. Le Formal, M. Gratzel, Chem. Mater. 21 (2009) 2862.
[32] M.A. Gelesky, A.P. Umpierre, G. Machado, R.R.B. Correia, W.C. Magno, J. Morais, G. Ebeling, J. Dupont, J. Am. Chem. Soc. 127 (2005) 4588.
[33] Z.R. Dai, Z.W. Pan, Z.L. Wang, Adv. Funct. Mater. 13 (2003) 9.
[34] K. Wasa, M. Kitabatake, H. Adachi, Thin Film Materials Technology: Sputtering of Compound Materials, William Andrew, Inc., United States, 2004.
[35] H. Wender, L.F. de Oliveira, P. Migowski, A.F. Feil, E. Lissner, M.H.G. Prechtl, S.R. Teixeira, J. Dupont, J. Phys. Chem. C 114 (2010) 11764.
[36] T. Torimoto, K. Okazaki, T. Kiyama, K. Hirahara, N. Tanaka, S. Kuwabata, Appl. Phys. Lett. 89 (2006), 243117.
[37] W.R. Grove, Philos. Trans. R. Soc. Lond. 142 (1852) 87.
[38] K. Wasa, S. Hayakawa, Handbook of Sputter Deposition Technology: Principles, Technology and Applications, Noyes Publications, Westwood, NJ, USA, 1992.
[39] K.-Y. Chan, B.-S. Teo, J. Mater. Sci. 40 (2005) 5971.
[40] P. Gao, L.J. Meng, M.P. dos Santos, V. Teixeira, M. Andritschky, Thin Solid Films 377–378 (2000) 557.
[41] M. Wagener, B. Günther, J. Magn. Magn. Mater. 201 (1999) 41.
[42] H. Wender, L.F. de Oliveira, A.F. Feil, E. Lissner, P. Migowski, M.R. Meneghetti, S.R. Teixeira, J. Dupont, Chem. Commun. 46 (2010) 7019.
[43] G.X. Ye, Q.R. Zhang, C.M. Feng, H.L. Ge, Z.K. Jiao, Phys. Rev. B 54 (1996) 14754.
[44] G.X. Ye, C.M. Geng, Z.R. Zhang, H.L. Ge, X.J. Zhang, Chin. Phys. Lett. 13 (1996) 772.
[45] H.L. Ge, C.M. Feng, G.X. Ye, Y.H. Ren, J.K. Jiao, J. Appl. Phys. 82 (1997) 5469.
[46] G.X. Ye, T. Michely, V. Weidenhof, I. Friedrich, M. Wuttig, Phys. Rev. Lett. 81 (1998) 622.
[47] C.M. Feng, H.L. Ge, M.R. Tong, G.X. Ye, Z.K. Jiao, Thin Solid Films 342 (1999) 30.
[48] C.W. Wu, H. Conrad, Int. J. Mod. Phys. B 13 (1999) 1713.
[49] X.M. Tao, Y.W. Zeng, C.M. Feng, Z.K. Jiao, G.X. Ye, Acta Phys. Sin. 49 (2000) 2235.
[50] J.S. Jin, A.G. Xia, G.X. Ye, Acta Phys. Sin. 51 (2002) 2144.
[51] B. Yang, A.G. Xia, J.S. Jin, Q.L. Ye, Y.F. Lao, Z.K. Jiao, G.X. Ye, J. Phys.: Condens. Matter 14 (2002) 10051.
[52] Q.L. Ye, X.J. Xu, P.G. Cai, A.G. Xia, G.X. Ye, Phys. Lett. A 318 (2003) 457.
[53] Q.L. Ye, S.J. Yu, J.S. Jin, G.X. Ye, Chin. Phys. Lett. 20 (2003) 1109.
[54] J.Q. Mai, W.G. Fruh, Meas. Sci. Technol. 15 (2004) 170.
[55] S.J. Yu, Y.J. Zhang, J.X. Chen, H.L. Ge, Surf. Rev. Lett. 13 (2006) 779.
[56] Y.J. Zhang, S.J. Yu, H.L. Ge, L.N. Wu, Y.J. Cui, Acta Phys. Sin. 55 (2006) 5444.
[57] X.J. Xu, Q.L. Ye, G.X. Ye, Phys. Lett. A 361 (2007) 429.
[58] Y.J. Zhang, S.J. Yu, Int. J. Mod. Phys. B 23 (2009) 3147.
[59] E.F. Borra, O. Seddiki, R. Angel, D. Eisenstein, P. Hickson, K.R. Seddon, S.P. Worden, Nature 447 (2007) 979.
[60] J. Dupont, R.F. de Souza, P.A.Z. Suarez, Chem. Rev. 102 (2002) 3667.
[61] M.C. Buzzeo, R.G. Evans, R.G. Compton, Chem. Phys. Chem. 5 (2004) 1106.
[62] C.E. Song, Chem. Commun. (2004) 1033.
[63] R.A. Reich, P.A. Stewart, J. Bohaychick, J.A. Urbanski, Lubr. Eng. 59 (2003) 16.
[64] R.F. de Souza, J.C. Padilha, R.S. Goncalves, J. Dupont, Electrochem. Commun. 5 (2003) 728.
[65] M. Gorlov, L. Kloo, Dalton Trans. (2008) 2655.
[66] J.L. Anderson, D.W. Armstrong, Anal. Chem. 75 (2003) 4851.
[67] C.C. Cassol, A.P. Umpierre, G. Ebeling, B. Ferrera, S.S.X. Chiaro, J. Dupont, Int. J. Mol. Sci. 8 (2007) 593.
[68] S. Park, R.J. Kazlauskas, Curr. Opin. Biotechnol. 14 (2003) 432.
[69] R.R. Deshmukh, R. Rajagopal, K.V. Srinivasan, Chem. Commun. (2001) 1544.
[70] J. Dupont, G.S. Fonseca, A.P. Umpierre, P.F.P. Fichtner, S.R. Teixeira, J. Am. Chem. Soc. 124 (2002) 4228.
[71] F. Endres, S.Z. El Abedin, Chem. Commun. (2002) 892.
[72] Y. Zhou, M. Antonietti, J. Am. Chem. Soc. 125 (2003) 14960.
[73] M. Green, P. Rahman, D. Smyth-Boyle, Chem. Commun. (2007) 574.
[74] M. Antonietti, D.B. Kuang, B. Smarsly, Z. Yong, Angew. Chem. Int. Ed. 43 (2004) 4988.
[75] P. Migowski, J. Dupont, Chem. Eur. J. 13 (2007) 32.
[76] A. Elaiwi, P.B. Hitchcock, K.R. Seddon, N. Srinivasan, Y.M. Tan, T. Welton, J.A. Zora, J. Chem. Soc. Dalton Trans. (1995) 3467.
[77] S. Saha, S. Hayashi, A. Kobayashi, H. Hamaguchi, Chem. Lett. 32 (2003) 740.
[78] A. Mele, C.D. Tran, S.H.D. Lacerda, Angew. Chem. Int. Ed. 42 (2003) 4364.
[79] F.C. Gozzo, L.S. Santos, R. Augusti, C.S. Consorti, J. Dupont, M.N. Eberlin, Chem. Eur. J. 10 (2004) 6187.
[80] P. Migowski, D. Zanchet, G. Machado, M.A. Gelesky, S.R. Teixeira, J. Dupont, Phys. Chem. Chem. Phys. 12 (2010) 6826.
[81] C.W. Scheeren, G. Machado, S.R. Teixeira, J. Morais, J.B. Domingos, J. Dupont, J. Phys. Chem. B 110 (2006) 13011.
[82] P. Migowski, G. Machado, S.R. Texeira, M.C.M. Alves, J. Morais, A. Traverse, J. Dupont, Phys. Chem. Chem. Phys. 9 (2007) 4814.
[83] T. Gutel, J. Garcia-Anton, K. Pelzer, K. Philippot, C.C. Santini, Y. Chauvin, B. Chaudret, J.M. Basset, J. Mater. Chem. 17 (2007) 3290.
[84] E. Redel, R. Thomann, C. Janiak, Inorg. Chem. 47 (2008) 14.
[85] E. Redel, R. Thomann, C. Janiak, Chem. Commun. (2008) 1789.
[86] G.S. Fonseca, G. Machado, S.R. Teixeira, G.H. Fecher, J. Morais, M.C.M. Alves, J. Dupont, J. Colloid Interface Sci. 301 (2006) 193.
[87] T. Gutel, C.C. Santini, K. Philippot, A. Padua, K. Pelzer, B. Chaudret, Y. Chauvin, J.M. Basset, J. Mater. Chem. 19 (2009) 3624.
[88] J. Dupont, Acc. Chem. Res. 44 (2011) 1223.
[89] K.I. Okazaki, T. Kiyama, K. Hirahara, N. Tanaka, S. Kuwabata, T. Torimoto, Chem. Commun. (2008) 691.
[90] T. Suzuki, K. Okazaki, T. Kiyama, S. Kuwabata, T. Torimoto, Electrochemistry 77 (2009) 636.
[91] Y. Hatakeyama, M. Okamoto, T. Torimoto, S. Kuwabata, K. Nishikawa, J. Phys. Chem. C 113 (2009) 3917.
[92] Y. Hatakeyama, S. Takahashi, K. Nishikawa, J. Phys. Chem. C 114 (2010) 11098.
[93] T. Suzuki, S. Suzuki, Y. Tomita, K. Okazaki, T. Shibayama, S. Kuwabata, T. Torimoto, Chem. Lett. 39 (2010) 1072.
[94] T. Suzuki, K.-i. Okazaki, S. Suzuki, T. Shibayama, S. Kuwabata, T. Torimoto, Chem. Mater. 22 (2010) 5209.
[95] H. Wender, P. Migowski, A.F. Feil, L.F. de Oliveira, M.H.G. Prechtl, R. Leal, G. Machado, S.R. Teixeira, J. Dupont, Phys. Chem. Chem. Phys. 13 (2011) 13552.
[96] E. Vanecht, K. Binnemans, J.W. Seo, L. Stappers, J. Fransaer, Phys. Chem. Chem. Phys. 13 (2011) 13565.
[97] E. Vanecht, K. Binnemans, S. Patskovsky, M. Meunier, J.W. Seo, L. Stappers, J. Fransaer, Phys. Chem. Chem. Phys. 14 (2012) 5662.
[98] H. Wender, R.V. Gonçalves, A.F. Feil, P. Migowski, F.S. Poletto, A.R. Pohlmann, J. Dupont, S.R. Teixeira, J. Phys. Chem. C 115 (2011) 16362.
[99] Y. Hatakeyama, T. Morita, S. Takahashi, K. Onishi, K. Nishikawa, J. Phys. Chem. C 115 (2011) 3279.
[100] Y. Shishino, T. Yonezawa, K. Kawai, H. Nishihara, Chem. Commun. 46 (2010) 7211.
[101] K. Okazaki, T. Kiyama, T. Suzuki, S. Kuwabata, T. Torimoto, Chem. Lett. 38 (2009) 330.

[102] T. Tsuda, T. Kurihara, Y. Hoshino, T. Kiyama, K. Okazaki, T. Torimoto, S. Kuwabata, Electrochemistry 77 (2009) 693.
[103] E.C. da Silva, M.G.A. da Silva, S.M.P. Meneghetti, G. Machado, M. Alencar, J.M. Hickmann, M.R. Meneghetti, J. Nanopart. Res. 10 (2008) 201.
[104] H. Wender, M.L. Andreazza, R.R.B. Correia, S.R. Teixeira, J. Dupont, Nanoscale 3 (2011) 1240.
[105] Y. Hatakeyama, K. Onishi, K. Nishikawa, RSC Adv. 1 (2011) 1815.
[106] S. Suzuki, Y. Ohta, T. Kurimoto, S. Kuwabata, T. Torimoto, Phys. Chem. Chem. Phys. 13 (2011) 13585.
[107] M. Nie, K. Sun, D.D. Meng, J. Appl. Phys. 106 (2009), 054314.
[108] C. Gutierrez-Wing, R. Esparza, C. Vargas-Hernandez, M.E.F. Garcia, M. Jose-Yacaman, Nanoscale 4 (2012) 2281.
[109] K. Wegner, B. Walker, S. Tsantilis, S.E. Pratsinis, Chem. Eng. Sci. 57 (2002) 1753.
[110] R. Bussamara, D. Eberhardt, A.F. Feil, P. Migowski, H. Wender, D. Moraes, G. Machado, R.M. Papaleo, S.R. Teixeira, J. Dupont, Chem. Commun. (2013), http://dx.doi.org/10.1039/C1032CC38737A.
[111] K. Okazaki, J. Sakuma, J. Yasui, S. Kuwabata, K. Hirahara, N. Tanaka, T. Torimoto, Chem. Lett. 40 (2011) 84.
[112] C.-H. Liu, B.-H. Mao, J. Gao, S. Zhang, X. Gao, Z. Liu, S.-T. Lee, X.-H. Sun, S.-D. Wang, Carbon 50 (2012) 3008.
[113] K. Yoshii, T. Tsuda, T. Arimura, A. Imanishi, T. Torimoto, S. Kuwabata, RSC Adv. 2 (2012) 8262.
[114] H. Yoshida, K. Kawamoto, H. Kubo, T. Tsuda, A. Fujii, S. Kuwabata, M. Ozaki, Adv. Mater. 22 (2010) 622.
[115] T. Tsuda, K. Yoshii, T. Torimoto, S. Kuwabata, J. Power Sources 195 (2010) 5980.
[116] Y. Oda, K. Hirano, K. Yoshii, S. Kuwabata, T. Torimoto, M. Miura, Chem. Lett. 39 (2010) 1069.
[117] T. Kameyama, Y. Ohno, T. Kurimoto, K. Okazaki, T. Uematsu, S. Kuwabata, T. Torimoto, Phys. Chem. Chem. Phys. 12 (2010) 1804.
[118] S.C. Hamm, R. Shankaran, V. Korampally, S. Bok, S. Praharaj, G.A. Baker, J.D. Robertson, B.D. Lee, S. Sengupta, K. Gangopadhyay, S. Gangopadhyay, ACS Appl. Mater. Interfaces 4 (2012) 178.
[119] C. Kolbeck, T. Cremer, K.R.J. Lovelock, N. Paape, P.S. Schulz, P. Wasserscheid, F. Maier, H.P. Steinruck, J. Phys. Chem. B 113 (2009) 8682.